DINAME 2019 - Proceedings of the XV International Symposium on Dynamic Problems of Mechanics,
M.A. Savi, T.G. Ritto and W.M. Bessa (Editors), ABCM, Buzios, RJ, Brazil, March 10th to 15th, 2019

Sliding Mode Control Strategies for Flexible Rotating Systems

Adriano Domeny dos Santos [1], Agenor de Toledo Fleury [1]

[1] Escola Politécnica da Universidade de São Paulo, Department of Mechanical Engineering, São Paulo, Brazil

Abstract: The aim of this work is to present the results of the implementation of a robust control technique – sliding mode control – to stabilize a Jeffcott rotor orbit by means of shaft traction actuation, where the rotor is subject to lateral impact and rubbing. The rotor eccentricity is modeled as uncertain variable. As a result of simulations, some orbits diagrams are achieved, indicating the system trajectories from arbitrary conditions to reach the desired orbit. This study contributes to a better understanding of how to mitigate rubbing and impact phenomena in real problems involving drilling systems for oil and gas wells.

Keywords: Jeffcott rotor, rubbing, impact, sliding mode and shaft traction

INTRODUCTION

A common situation in rotor dynamics is the lateral movement caused by rotor eccentricity. If there are others rigid elements in the rotor vicinity, lateral movements usually cause impacts and rubbing. The combination of these phenomena leads to the emergence of nonlinear behaviors such as backward rub, forward rub, periodic and quasi-periodic impacts, and chaotic movements. Specially in drilling systems for oil and gas industry, these rotor phenomena are undesired because they accelerate the wear of system parts and reduce the drilling process efficiency.

In Choy and Padovan (1987), rubbing phenomenon was studied in a rotor-case system, starting from a nonlinear dynamic model for a Jeffcott rotor. In Li and Paidoussis (1994), a theoretical study of the rubbing was carried out, taking into account the factors of most influence of this phenomenon: gap between rotor and stator, rotor eccentricity, and dry friction in the contact between rotor-casing elements. In Jonusas and Juzenas (2010), a study was carried out about occurrence of rubbing in the rotor of an industrial compressor. In Fonsega (2013), a way of limiting the rotor orbit inside a stator by inserting lateral contact pins was proposed. Finally, in Fernandes (2017), the sliding modes control technique with variable boundary layer was developed for the stabilization of systems subject to torsional vibrations. Additionally, artificial intelligence techniques were proposed in order to return the tracking performance of the controller, lost by the soft functions used into boundary layer.

The aim of this work is to present control strategies based on sliding mode technique, to mitigate the contact between rotor and stator for a Jeffcott rotor model, with a focus on shaft traction. This study contributes to a better understanding of how to mitigate rubbing and impact phenomena in real problems involving drilling systems for oil and gas wells.

The rotating system of the drilling process consists of a rotary table (an electric motor); an extremely thin cylindrical column, for transmission of the rotating energy to the drill; the Bottom Holly Assemble (BHA); and the drill. BHA, in turn, has the role of maintaining the column in a traction regime, thus reducing lateral impacts of the column with the hole wall, and at the same time generating weight on the drill bit. Therefore, the system is designed so that the neutral point, which separates the traction and compression regimes along the column, lies along the length of the BHA. Because it is partially compressed, and because of its eccentricity, the BHA is more exposed to lateral shocks. Inspired by the actual drilling system, the Jeffcott rotor was modeled considering an extremely slender shaft.

DYNAMIC MODEL

For this study, the rotating system is modeled as a Jeffcott rotor, as illustrated in Fig. 1.

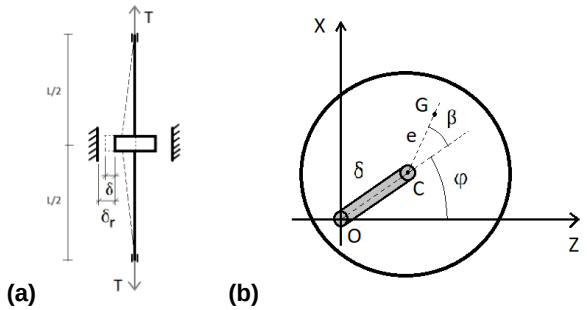

Figure 1 – Jeffcott rotor: (a) Lateral view; (b) Bottom view.

In Figure 1a, T is the shaft traction actuation and δ_r is rotor-casing clearance. In Fig. 1b, δ is the radial displacement of the geometric center C, and G is the mass center of the rotor.

Table 1 shows the dimensions of the rotor and shaft, as well as some properties of the material that constitute the system elements, and dynamic model parameters.

Table 1 – Dimensions of the rotor and shaft, property materials and dynamic parameters

Parameters	Symbol	Values
Shaft length (mm)	L	2500
Shaft diameter (mm)	d	3
Rotor diameter (mm)	D_r	200
Rotor thickness (mm)	L_r	20
Rotor eccentricity estimative (mm)	$\hat{e}$	5
Shaft elasticity modulus (GPa)	E	205
Rotor mass (kg)	m	4.9
Rotor angular velocity (rad/s)	Ω	2π
Rotor-casing clearance (mm)	δ_r	10

For simulation purposes, total angular velocity of the rotor, Ω, was considered constant. Consequently $\Omega t = \varphi + \beta$, according to parameters in Fig.1b.

Mathematical Equations

The system dynamics is described by equations obtained from Lagrangian formulation, and is presented in Eq. (1). It is written in state space form.

$$\begin{bmatrix} \dot{\delta} \\ \dot{\beta} \\ \dot{v}_\delta \\ \dot{w}_\beta \end{bmatrix} = \begin{bmatrix} v_\delta \\ w_\beta \\ \left(\Omega - w_\beta\right)^2 \delta - \frac{b}{m} v_\delta + e\Omega^2 \cos(\beta) - \frac{F_n}{m} \\ \left(\frac{2v_\delta}{\delta} + \frac{b}{m}\right)\left(\Omega - w_\beta\right) - \frac{e\Omega^2 \sin(\beta)}{\delta} + \frac{\mu F_n}{m\delta} \operatorname{sign}(\Omega) \end{bmatrix} + \begin{bmatrix} 0 \\ 0 \\ -\frac{\delta}{m} \\ 0 \end{bmatrix} k_e \tag{1}$$

In Equation (1), $v_\delta = \dot{\delta}$ and $w_\beta = \dot{\beta}$ are state variables, b is the lateral damping coefficient, F_n is the impact force, and k_e is the lateral stiffness and control variable.

Equations (2) and (3) correspond respectively to the total kinetic energy and potential energy of the system:

$$T_c = \frac{1}{2} m \left[\left(\dot{x} + e\Omega\cos(\varphi + \beta)\right)^2 + \left(\dot{z} - e\Omega\sin(\varphi + \beta)\right)^2 \right] \tag{2}$$

$$U = \frac{1}{2} k_e(t) \left[x^2 + z^2 \right] \tag{3}$$

Variables x and z correspond to the position of the geometric center C. Applying these expressions to the Lagrangian equations leads to the following:

$$\frac{d}{dt}\left(\frac{\partial L}{\partial \dot{x}}\right) - \frac{\partial L}{\partial x} = -b\dot{x} + F_{nx} \Rightarrow \frac{d}{dt}\left(\frac{\partial T_c}{\partial \dot{x}}\right) - \frac{\partial U}{\partial x} = -b\dot{x} + F_{nx} \tag{4}$$

$$\frac{d}{dt}\left(\frac{\partial L}{\partial \dot{z}}\right) - \frac{\partial L}{\partial z} = -b\dot{z} + F_{nz} \Rightarrow \frac{d}{dt}\left(\frac{\partial T_c}{\partial \dot{z}}\right) - \frac{\partial U}{\partial z} = -b\dot{z} + F_{nz} \tag{5}$$

The forces F_{nx} and F_{nz} are the components of rubbing and impact normal forces (F_n) summed. From Eq. (4) and (5), we obtain the system motion equations:

$$m\ddot{x} + b\dot{x} + k(t)x = m\Omega^2 e\sin(\Omega t) - F_n\sin(\varphi) - \mu F_n \text{sign}(\Omega)\cos(\varphi) \tag{6}$$

$$m\ddot{z} + b\dot{z} + k(t)z = m\Omega^2 e\cos(\Omega t) - F_n\cos(\varphi) + \mu F_n \text{sign}(\Omega)\sin(\varphi) \tag{7}$$

By substituting $x = \delta\cos(\varphi) = \delta\cos(\Omega t - \beta)$ and $z = \delta\sin(\varphi) = \delta\sin(\Omega t - \beta)$ in Eq. (6) and (7), we obtain Eq. (8) and (9):

$$\ddot{\delta} = \left[(\Omega - \dot{\beta})^2 - \frac{k_e(t)}{m}\right]\delta - \frac{b}{m}\dot{\delta} + e\Omega^2\cos(\beta) - \frac{F_n}{m} \tag{8}$$

$$\ddot{\beta} = \left(\frac{2\dot{\delta}}{\delta} + \frac{b}{m}\right)(\Omega - \dot{\beta}) - \frac{e\Omega^2}{\delta}\sin(\beta) + \frac{\mu F_n}{m\delta}\text{sign}(\Omega) \tag{9}$$

By rewriting Eq. (8) and (9) in the form of a state equation, we obtain Eq. (1).

The value k_e in Eq. (8) depends on shaft boundary conditions, and is a function of traction variable T, as in Eq. (10) and (11).

$$k_e \cong \frac{48EI}{L^3} + \frac{4}{L}\Delta T \tag{10}$$

$$\Delta T = \frac{E\pi d^2}{4}\frac{\Delta L}{L} = \frac{E\pi d^2}{4}\varepsilon \tag{11}$$

The impact force is modeled as in Eq. (12), where $K_r = 10^8 N/m$.

$$F_n = \begin{cases} 0 & , \delta < \delta_r \\ K_r(\delta - \delta_r) & , \delta \geq \delta_r \end{cases} \tag{12}$$

Equation (13) presents Eq. (1) in a matrix form. In addition, Eq. (13) shows the output variable as a function of state variables.

$$\begin{cases} \dot{Z} = f(Z) + g(Z)k_e \\ y = \delta = [1 \quad 0 \quad 0 \quad 0]Z = CZ \end{cases} \tag{13}$$

To summarize, the model input variable is the lateral stiffness, k_e, and the output is the radial position of the rotor geometric center, δ.

For defining the control law, Eq. (13) is rewritten in normal form (Li and Slotine, 1991), as in Eq. (14). The system has degree $n = 4$ and relative degree $r = 2$.

$$\ddot{y} = a(X) + \bar{b}(X)k_e \tag{14}$$

$$a(X) = (\Omega - w_\beta)^2\delta - \frac{b}{m}v_\delta + e\Omega^2\cos(\beta) - \frac{F_n}{m}$$

$$\bar{b}(X) = -\frac{\delta}{m}$$

$$X = \begin{bmatrix} y \\ \dot{y} \\ \beta \\ w_\beta \end{bmatrix} = \begin{bmatrix} \delta \\ v_\delta \\ \beta \\ w_\beta \end{bmatrix} = \begin{bmatrix} 1 & 0 & 0 & 0 \\ 0 & 0 & 1 & 0 \\ 0 & 1 & 0 & 0 \\ 0 & 0 & 0 & 1 \end{bmatrix}\begin{bmatrix} \delta \\ \beta \\ v_\delta \\ w_\beta \end{bmatrix} = \begin{bmatrix} C_1 \\ C_3 \\ A_{01} \end{bmatrix}Z$$

The new coordinate system for the normal form is X, where $C_1 = [1 \;\; 0 \;\; 0 \;\; 0]$, $C_3 = [0 \;\; 0 \;\; 1 \;\; 0]$, and A_{01} is such that:

$$A_{01} = \begin{bmatrix} 0 & 1 & 0 & 0 \\ 0 & 0 & 0 & 1 \end{bmatrix}$$

CONTROL LAW

Once we know that the system relative degree is $r = 2$, sliding variable s is defined as in Eq. (15).

$$s(y,t) = \left(\frac{d}{dt} + \lambda\right)^{r-1}(y - y_d) = \left(\dot{\delta} - \dot{\delta}_d\right) + \lambda\left(\delta - \delta_d\right) \tag{15}$$

In Equation (15), λ is a control parameter and $y_d = \delta_d$ is the desired trajectory, as in Eq. (16).

$$\delta_d(t) = \delta_{final} - \left(\delta_{final} - \frac{\delta_r}{2}\right)\exp\left(-\alpha_\delta t\right) \tag{16}$$

In Equation (16), δ_r is the rotor-casing clearance, δ_{final} is the desired final radial position of the geometric center, and α_δ is a predefined exponential decay parameter.

Equations (17) and (18) display, respectively, the chosen Lyapunov function for the system and a sliding condition for defining the control law.

$$V = \frac{1}{2}s^2 \tag{17}$$

$$\dot{V} = \frac{1}{2}\frac{d}{dt}s^2 < \left(\dot{\Phi}_{bd} - \eta\right)|s| \text{ for } |s| \geq \Phi_{bd} \tag{18}$$

The sliding condition is defined for a variable boundary layer Φ_{bd} and an appropriate η value so that $\dot{V} < 0$ for $|s| \geq \Phi_{bd}$. The variable boundary layer acts as a low pass filter, eliminating the occurrence of chattering over the actuator.

We define the control law to satisfy the sliding condition, according to Eq. (19). This fact is demonstrated in the Appendix.

$$k_e = \frac{1}{\bar{b}(X)}\left[-\hat{a}(X) - \bar{K}(X, X_d)\,\text{sat}\left(\frac{s}{\Phi_{bd}}\right) + \ddot{\delta}_d - \lambda\left(v_\delta - \dot{\delta}_d\right)\right] \tag{19}$$

$$\hat{a}(X) = \left(\Omega - w_\beta\right)^2 \delta - \frac{b}{m}v_\delta + \hat{e}\Omega^2\cos(\beta)$$

In Equation (19), $\hat{a}(X)$ is an estimative of $a(X)$ based on $\hat{e}$, an approximation of e, which is uncertain. In the expression of $\hat{a}(X)$, the impact force F_n is omitted because it is different from zero only when an impact occur. On the other hand, the expression $\bar{K}(X, X_d)\,\text{sat}\left(s/\Phi_{bd}\right)$ is the switching term of the sliding mode control, and $\bar{K}(X, X_d)$ is the gain defined as in Eq. 22.

The advantage of using a variable boundary layer is to eliminate chattering at motor input, while having the disadvantage of precision loss. The sliding condition ensures that the sliding variable s tends to the boundary layer, but does not guarantee that the variable s tends to zero within the layer.

The function $\sigma(\upsilon) = \text{sat}(\upsilon)$ is a hyperbolic tangent function, given by Eq. 20 and illustrated in Fig. 2.

$$\sigma(\upsilon) = \text{sat}(\upsilon) = \tanh(\pi\upsilon) \tag{20}$$

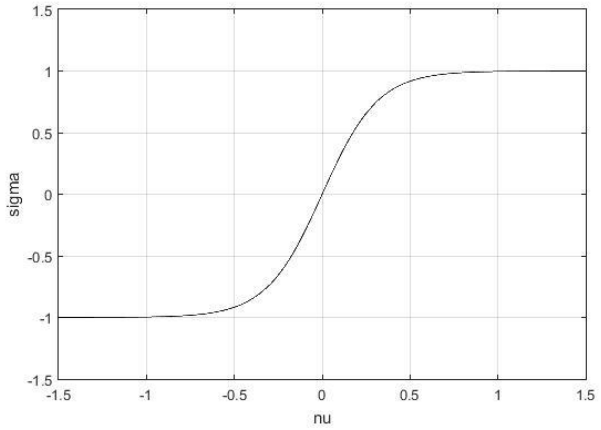

Figure 2 – Function $\sigma(\upsilon) = \text{sat}(\upsilon)$.

The gain $\bar{K}(X, X_d)$ is obtained as follows (Li and Slotine, 1991):

1. The function $F(X)$ is defined considering the absence of impacts, so that:

$$F(X) \geq |\hat{a} - a| = |\Delta a| \cong \left|\frac{\partial \hat{a}}{\partial \hat{e}}\right| |\Delta e| = \Omega^2 |\cos(\beta)| |\Delta e_{max}|$$

$$F(X) = \sigma_F \Omega^2 |\cos(\beta)| |\Delta e_{max}| \text{ for } \sigma_F \geq 1 \tag{21}$$

2. The function $K(X) = F(X) + \eta$ is defined and corresponds to the switching gain for the case of null boundary layer.
3. Finally, the gain $\bar{K}(X, X_d)$ is defined as in Eq. 22. The variable Φ_{bd} corresponds to the boundary layer in contraction or expansion.

$$\bar{K}(X, X_d) = K(X) - K(X_d) + \lambda \Phi_{bd} \tag{22}$$

Time evolution of Φ_{bd} is described by Eq. (23), as in Li and Slotine, 1991.

$$\dot{\Phi}_{bd} = -\lambda \Phi_{bd} + K(X_d) \tag{23}$$

NUMERICAL IMPLEMENTATION

The motion equations were integrated by means of the fourth-order Runge-Kutta method, with fixed step $\Delta t = 10^{-4}\,s$. The control parameter η was estimated considering the reach time $t_{sld} = 7\,s$:

$$\eta = \frac{|s(t) - s(t_0 = 0)|}{t_{sld}} \cong \frac{|s(t_0 = 0)|}{t_{sld}}$$

$$\eta \cong \frac{\left|\left(\dot{\delta}(0) - \dot{\delta}_d(0)\right) + \lambda\left(\delta(0) - \delta_d(0)\right)\right|}{t_{sld}} = \frac{\left|(0-0) + \lambda\left(1.0 \times 10^{-3} - 0\right)\right|}{7} = 3.2 \times 10^{-4}\,\frac{m}{s^2}$$

The parameter λ, set to $\lambda = 2\omega_n$, is the cutting frequency of the low-pass filter that eliminates chattering. The parameter ω_n is the highest natural frequency of the system lateral vibration.

$$\omega_n = \sqrt{\frac{K_e}{m}} = \sqrt{\frac{1}{m} 48 \frac{EI}{L^3}} \cong 0.7 \text{rad/s}$$

CONTROL LAW ROBUSTNESS

It is known that the variable boundary layer acts as a low pass filter, thus eliminating the chattering at the input of the actuator. On the other hand, the sliding condition with variable boundary layer in Eq. (18) guarantees that the sliding variable s tends to the layer, but does not guarantee that it tends to zero within the layer (Li and Slotine, 1991). This makes the tracking of the desired trajectory less precise.

In a brief qualitative analysis, an increase of σ_F corresponds to an increase of the control robustness, since the $F(X) \geq |\hat{a} - a|$ guarantees sliding condition in Eq. 18. On the other hand, from Eq. 23, it can be shown that, in steady state, the layer Φ_{bd} satisfies:

$$\Phi_{bd} = \frac{K(X_d)}{\lambda} = \frac{F(X_d) + \eta}{\lambda} \tag{24}$$

From Equation (24), one can conclude that an increase in the parameter σ_F implies an increase of the boundary layer width Φ_{bd} in steady state, which leads to a loss of tracking precision, and consequently to an increase in the impact chance. In turn, reducing the value of δ_{final} reduces the chance of rotor lateral impact, but leads to an increase in the actuation effort.

It is important to emphasize that the main objective of the present study is not to ensure that the output variable δ follows the desired trajectory, but only to ensure that it avoids the lateral impact of the rotor with the casing during the movement, taking into account actuation effort. In other words, the condition of the Eq. (25) must be satisfied.

$$0 < \delta < \delta_r \tag{25}$$

Considering initially $\delta > 0$, one concludes that $s = \lambda(\delta - \delta_{final}) > \lambda(0 - \delta_{final}) = -\lambda\delta_{final}$. It implies that, if $|s| \geq \Phi_{bd}$, Φ_{bd} must be so that:

$$-\Phi_{bd} > -\lambda\delta_{final} \Leftrightarrow \Phi_{bd} < \lambda\delta_{final} \tag{26}$$

Equation (26) guarantees that, in steady state, $s > -\Phi_{bd} > -\lambda\delta_{final} \Rightarrow \delta > 0$.

From Equations (21), (24) and (26), in steady state, we get:

$$\frac{F(X_d) + \eta}{\lambda} < \lambda\delta_{final} \Leftrightarrow F(X_d) < \lambda^2\delta_{final} - \eta \Leftrightarrow \sigma_F\Omega^2 |\cos(\beta_d)||\Delta e_{max}| < \lambda^2\delta_{final} - \eta$$

$$|\Delta e_{max}| < \frac{\lambda^2\delta_{final} - \eta}{\sigma_F\Omega^2 |\cos(\beta_d)|} = \sigma_e \frac{\lambda^2\delta_{final} - \eta}{\sigma_F\Omega^2} \text{ for } \sigma_e = \frac{1}{|\cos(\beta_d)|} \geq 1$$

$$|\Delta e_{max}| = \frac{\sigma_e}{n_e} \frac{(\lambda^2\delta_{final} - \eta)}{\sigma_F\Omega^2} \text{ for } \sigma_e = \frac{1}{|\cos(\beta_d)|} \geq 1 \text{ and } n_e > 1 \tag{27}$$

Considering now $\delta < \delta_r$, one concludes that, in steady state, $s = \lambda(\delta - \delta_{final}) < \lambda(\delta_r - \delta_{final})$. It implies that, if $|s| \geq \Phi_{bd}$, Φ_{bd} must be so that:

$$\Phi_{bd} < \lambda(\delta_r - \delta_{final}) \tag{28}$$

Equation (28) guarantees that, in steady state, $s < \Phi_{bd} < \lambda(\delta_r - \delta_{final}) \Rightarrow \delta < \delta_r$. Equations (21), (24) e (28), in steady state, lead to:

$$\frac{F(X_d)+\eta}{\lambda} < \lambda(\delta_r - \delta_{final}) \Leftrightarrow F(X_d) < \lambda^2(\delta_r - \delta_{final}) - \eta \Leftrightarrow \sigma_F \Omega^2 \left|\cos(\beta_d)\right| \left|\Delta e_{max}\right| < \lambda^2(\delta_r - \delta_{final}) - \eta$$

$$\left|\Delta e_{max}\right| < \frac{\lambda^2(\delta_r - \delta_{final}) - \eta}{\sigma_F \Omega^2 \left|\cos(\beta_d)\right|} = \sigma_e \frac{\lambda^2(\delta_r - \delta_{final}) - \eta}{\sigma_F \Omega^2} \text{ for } \sigma_e = \frac{1}{\left|\cos(\beta_d)\right|} \geq 1$$

$$\left|\Delta e_{max}\right| = \frac{\sigma_e}{n_e} \frac{\left(\lambda^2(\delta_r - \delta_{final}) - \eta\right)}{\sigma_F \Omega^2} \text{ for } \sigma_e = \frac{1}{\left|\cos(\beta_d)\right|} \geq 1 \text{ and } n_e > 1 \tag{29}$$

One concludes from Eq. (27) and (29) that the condition in Eq. (25) is satisfied when:

$$\left|\Delta e_{max}\right| = \frac{\sigma_e}{n_e} \frac{1}{\sigma_F \Omega^2} \min\left\{\left(\lambda^2(\delta_r - \delta_{final}) - \eta\right), \left(\lambda^2 \delta_{final} - \eta\right)\right\} \text{ for } \sigma_e = \frac{1}{\left|\cos(\beta_d)\right|} \geq 1 \text{ and } n_e > 1 \tag{30}$$

From Equation (30), the highest value of $\left|\Delta e_{max}\right|$ is obtained if:

$$\delta_{final} = \frac{\delta_r}{2} \tag{31}$$

From Equation (31), one concludes that $\lambda^2(\delta_r - \delta_{final}) - \eta = \lambda^2 \delta_{final} - \eta$, and, from Eq. (30):

$$\left|\Delta e_{max}\right| = \frac{\sigma_e}{n_e} \frac{1}{\sigma_F \Omega^2} \left(\lambda^2 \left(\delta_r - \frac{\delta_r}{2}\right) - \eta\right) = \frac{\sigma_e}{n_e} \frac{\left(\lambda^2 \delta_r - 2\eta\right)}{2\sigma_F \Omega^2} \text{ for } \sigma_e = \frac{1}{\left|\cos(\beta_d)\right|} \geq 1 \text{ and } n_e > 1 \tag{32}$$

The robustness of the control law is analyzed for the predefined extreme conditions of uncertainty:

$$\hat{e} - \Delta e_{max} \leq e \leq \hat{e} + \Delta e_{max} \tag{33}$$

RESULTS

Initially, it was assumed that $e = \hat{e}$ and $\Omega = 2\pi \text{ rad/s}\,(60 \text{ rpm})$. Figure 3 shows the rotor orbits. In Fig.3a, the orbit corresponds to a constant lateral stiffness k_e, and in Fig.3b, the controller is activated. The desired final radial position is $\delta_{final} = 0.25\,\delta_r$, and initial coordinates are $z = 0.1\,\delta_r$ and $x = 0$. Comparing the two figures shows that the controller prevented successive collisions between the rotor and the casing.

Figure 4a shows the time evolution of sliding variable s and of boundary layer Φ_{bd}. In addition, Fig. 4b shows the desired trajectory and real trajectory of the rotor in time. It should be noticed that the sliding variable reached the boundary layer in a time interval shorter than the reach time $t_{sld} = 7$ s, a control project parameter. Moreover, the rotor reached the desired position in a time interval shorter than the reach time, as expected.

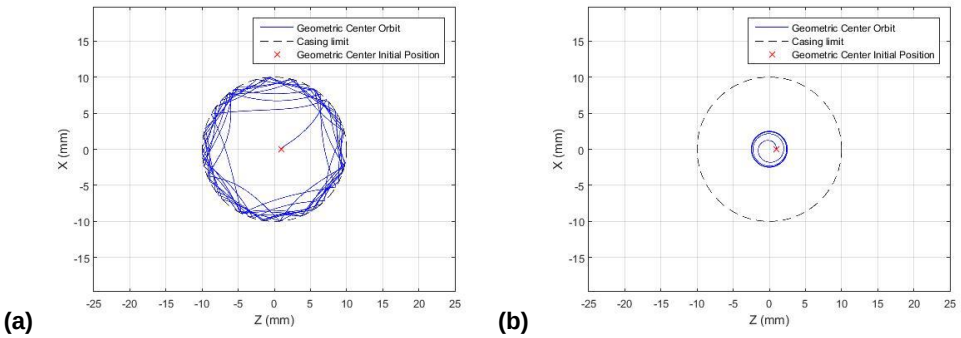

(a) **(b)**

Figure 3 – Rotor geometric center orbits. (a) Controller off. (b) Controller on.

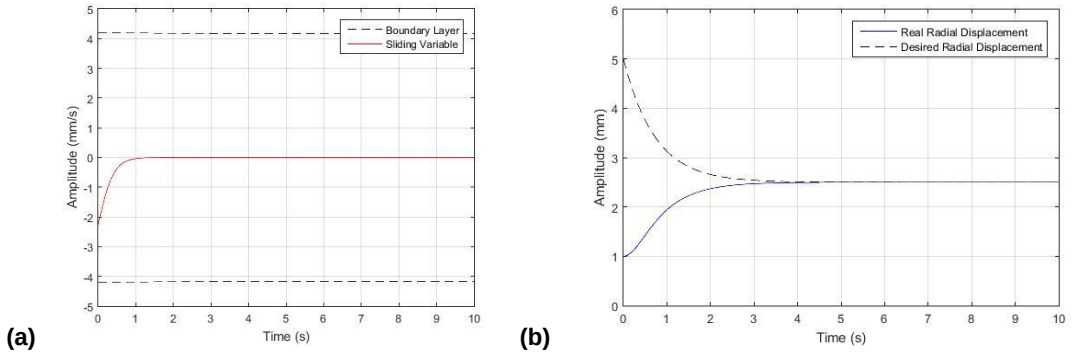

(a) **(b)**

Figure 4 – (a) Boundary layer and sliding variable in time. (b) Radial displacement of geometric center.

Figure 5 shows, for different angular velocities, the actuator performance through time evolution of shaft strain during the actuation. Average flow limit for steel is approximately 300 MPa. Considering shaft elasticity modulus $E = 205\ \text{GPa}$, as in Tab. 1, results in:

$$\Delta L_E = \frac{\sigma_E}{E} L = \frac{3\times10^8}{2.05\times10^{11}} 2500 \cong 3.7\ \text{mm}$$

Considering a security factor $n = 3$, one concludes that for $\Omega = 4\pi\ \text{rad/s}\ (120\ \text{RPM})$ and $\Omega = \frac{5\pi}{3}\ \text{rad/s}$ $(100\ \text{RPM})$, with respective strain peaks of $5\ \text{mm}$ and $3.5\ \text{mm}$, the actuation is impractical for a steel shaft with $2500\ \text{mm}$ in length. On the other hand, for $\Omega = \pi\ \text{rad/s}$ (30 RPM) and $\Omega = 2\pi\ \text{rad/s}$ (60 RPM) with respective strain peaks of approximately $0.3\ \text{mm}$ and $1.2\ \text{mm}$, the actuation is possible in the same conditions.

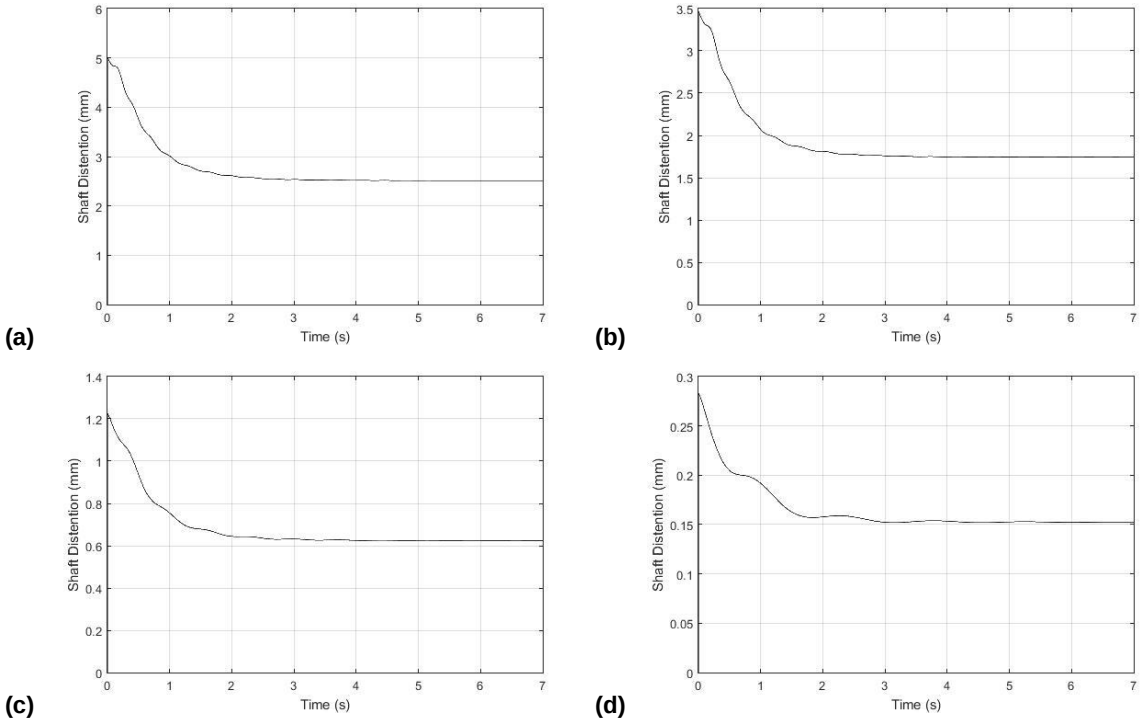

(a) **(b)** **(c)** **(d)**

Figure 5 – Time evolution of shaft distension: for (a) $\Omega = 4\pi\ \text{rad/s}$ (120 RPM), (b) $\Omega = \frac{5\pi}{3}\ \text{rad/s}$ (100 RPM), (c) $\Omega = 2\pi\ \text{rad/s}$ (60 RPM) and (d) $\Omega = \pi\ \text{rad/s}$ (30 RPM).

For the sake of studying the control robustness, let $e \neq \hat{e}$, $\hat{e} - \Delta e_{max} \leq e \leq \hat{e} + \Delta e_{max}$ and $\Omega = 2\pi\ \text{rad/s}$ $(60\ \text{rpm})$ be the new operating conditions.

Figure 6 is obtained by using Eq. 31 with the parameter values $\sigma_e = 1.2$ and $n_e = 1.01$, that satisfy Eq. 32. The value of Δe_{max} is obtained from Eq. 32:

$$|\Delta e_{max}| = \frac{\sigma_e}{n_e}\frac{\left(\lambda^2\delta_r - 2\eta\right)}{2\sigma_F\Omega^2} = \frac{1.2}{1.01}\frac{\left(1.4^2\times10^{-2} - 2\times2.15\times10^{-4}\right)}{2\times1.0\times(2\pi)^2} = 1.4\times10^{-4}\,\text{m} \cong 0.1\,\text{mm}$$

From Figure 6, one concludes that the conditions in Eq. (34) are satisfied for $\hat{e} - \Delta e_{max} \le e \le \hat{e} + \Delta e_{max}$:

$$\Delta L_{max} \le \frac{\Delta L_E}{n} \cong \frac{3.7}{3} \cong 1.23\,\text{mm} \text{ and } 0 < \delta < \delta_f = 10\,\text{mm} \tag{34}$$

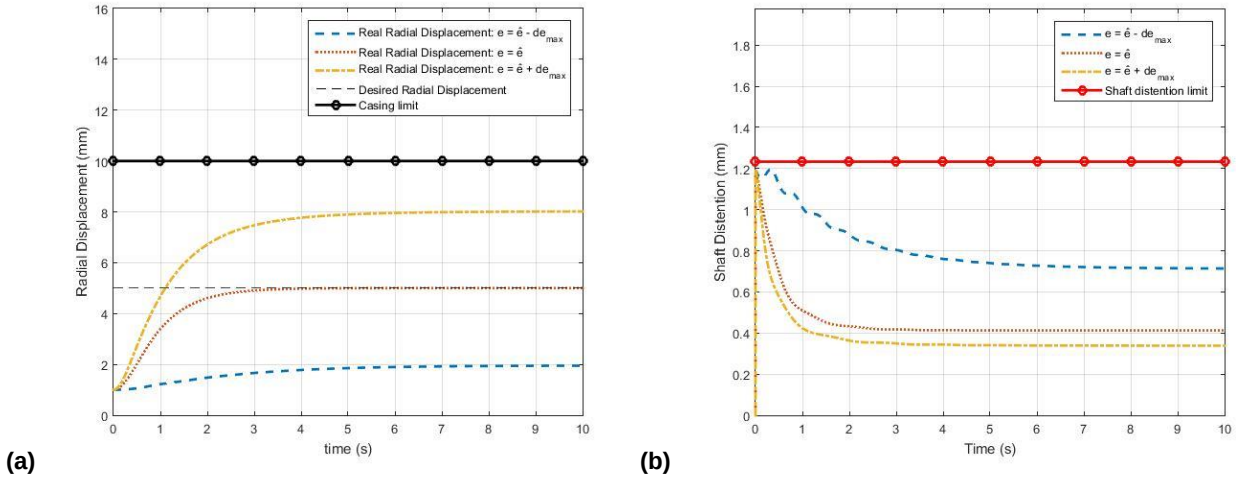

(a) **(b)**

Figure 6 – For $\Omega = 2\pi$ rad / s (60 RPM), $e = \hat{e} - \Delta e_{max}$, $e = \hat{e}$ and $e = \hat{e} + \Delta e_{max}$: (a) radial displacement; (b) shaft distension.

CONCLUSION

The aim of this work is to present a control strategy to mitigate the contact between rotor and casing for a simple Jeffcott rotor model, by means of shaft traction actuation. This study contributes to a better understanding of how to mitigate rubbing and impact phenomena in real problems involving drilling systems for oil and gas wells.

In simulations, the reach time project parameter is theoretically satisfied and collisions are successfully prevented by the controller in scenarios where $\Omega = 2\pi$ rad / s and $e = \hat{e}$. No chattering is observed over the actuator, and the control law is robust enough to avoid lateral impacts when $\hat{e} - \Delta e_{max} \le e \le \hat{e} + \Delta e_{max}$ and $e \neq \hat{e}$.

The maximum variation of the rotor eccentricity, Δe_{max} , without lateral impacts, is estimated for a given rotor speed Ω and a given clearance δ_r between the rotor and casing. To increase the value of Δe_{max} , it is necessary either to reduce the rotor speed Ω or increase the clearance value δ_r .

On the other hand, we show that, for test parameters resembling the real system, the adopted technique only works for low angular velocities, given that the actuation effort is unfeasible for speeds greater than $\Omega = 2\pi$ rad / s (60 RPM). Since the usual angular velocity in real drilling systems is around 100 RPM, it is concluded that shaft traction actuation is not enough. Consequently, we intend to study the combined actuation of traction and top motor (Santos and Fleury, 2017) at one end of the shaft in the near future.

REFERENCES

Choy, F., Padovan, J., 1989, "Non-linear transient analysis of rotor-casing rub events", Journal of Sound and Vibration, Vol.113, N. 3, pp. 529-545. Available in: http://www.sciencedirect.com/science/article/pii/S0022460X87801359.

Fernandes, J. M. M., 2017, "Controle Inteligente de Sistemas Subatuados com Aplicações em Problemas de Mecânica do Contato", Doctoral thesis – Universidade Federal do Rio Grande do Norte.

Fonseca, 2013, "Analyzing the use of active pins in safety bearing", Master dissertation – Pontifícia Universidade Católica do Rio de Janeiro.

Jonusas, E. J. R., Juzenas, K., 2010, "Analysis of some extreme situations in exploitation of complex rotary systems". Mechanics, ISSN, Vol. 81, N. 1, pp. 53-57.

Li, G. X., Paidoussis, M. P., 1994, "Impact phenomena of rotor-casing dynamical systems". Nonlinear Dynamics, ISSN, Vol. 5, N. 1, pp. 53-70. Available in https://doi.org/10.1007/BF00045080.

Li, W., Slotine, J. J., 1991, "Applied Nonlinear Control", Prentice Hall.

Santos, A. D., Fleury, A. T., 2017, "Sliding Mode Control of a Flexible Rotating System Subject to Concentrated Dry Friction". Proceedings of the COBEM 2017/24th ABCM International Congress of Mechanical Engineering. Curitiba, PR, paper 2455.

RESPONSIBILITY NOTICE

The authors are the only responsible for the printed material included in this paper.

APPENDIX

Control law in Eq. (19) satisfies sliding condition for variable boundary layer in Eq. (18).

Indeed, be $|s| \geq \Phi_{bd}$. It concludes that $s \cdot \text{sat}\left(\frac{s}{\Phi_{bd}}\right) \cong |s|$. So:

$$
\begin{aligned}
\dot{V} = \frac{1}{2}\frac{d}{dt}s^2 &= s\dot{s} \\
&= s\left[\ddot{\delta} - \ddot{\delta}_d + \lambda\left(\dot{\delta} - \dot{\delta}_d\right)\right] \\
&= s\left[a(X) + \bar{b}(X)k_e - \ddot{\delta}_d + \lambda\left(\dot{\delta} - \dot{\delta}_d\right)\right] \\
&= s\left[a(X) + \bar{b}(X)\frac{1}{\bar{b}(X)}\left(-\hat{a}(X) - \bar{K}(X, X_d)\,\text{sat}\left(\frac{s}{\Phi_{bd}}\right) + \ddot{\delta}_d - \lambda\left(v_\delta - \dot{\delta}_d\right)\right) - \ddot{\delta}_d + \lambda\left(\dot{\delta} - \dot{\delta}_d\right)\right] \\
&= s\left[a(X) - \hat{a}(X) - \bar{K}(X, X_d)\,\text{sat}\left(\frac{s}{\Phi_{bd}}\right) + \ddot{\delta}_d - \lambda\left(v_\delta - \dot{\delta}_d\right) - \ddot{\delta}_d + \lambda\left(\dot{\delta} - \dot{\delta}_d\right)\right] \\
&= s\left[a(X) - \hat{a}(X) - \bar{K}(X, X_d)\,\text{sat}\left(\frac{s}{\Phi_{bd}}\right)\right] \\
&= s\left[a(X) - \hat{a}(X)\right] - s\bar{K}(X, X_d)\,\text{sat}\left(\frac{s}{\Phi_{bd}}\right) \\
&= s\left[a(X) - \hat{a}(X)\right] - s\left[K(X) - K(X_d) + \lambda\Phi_{bd}\right]\text{sat}\left(\frac{s}{\Phi_{bd}}\right) \quad \text{(Eq. 22)} \\
&= s\left[a(X) - \hat{a}(X)\right] - s\left[K(X) - \dot{\Phi}_{bd}\right]\text{sat}\left(\frac{s}{\Phi_{bd}}\right) \quad \text{(Eq. 23)} \\
&= s\left[a(X) - \hat{a}(X)\right] - s\left[F(X) + \eta - \dot{\Phi}_{bd}\right]\text{sat}\left(\frac{s}{\Phi_{bd}}\right) \\
&\leq |s|\left|a(X) - \hat{a}(X)\right| - sF(X)\,\text{sat}\left(\frac{s}{\Phi_{bd}}\right) + s\left[\dot{\Phi}_{bd} - \eta\right]\text{sat}\left(\frac{s}{\Phi_{bd}}\right) \\
&= |s|\left|a(X) - \hat{a}(X)\right| - |s|F(X) + |s|\left[\dot{\Phi}_{bd} - \eta\right] \\
&= -|s|\left[F(X) - \left|a(X) - \hat{a}(X)\right|\right] + |s|\left[\dot{\Phi}_{bd} - \eta\right] \\
&\leq \left[\dot{\Phi}_{bd} - \eta\right]|s|
\end{aligned}
$$